Improving Temperature Accuracy for Rapid Thermal Processing at NIST

Speaker: Benjamin K. Tsai
National Institute of Standards and Technology
100 Bureau Drive Stop 8441
Gaithersburg, MD 20899-8441
Phone: (301) 975-2347
Fax: (301) 869-5700
Email: tsai@nist.gov

Authors: Benjamin K. Tsai and David P. DeWitt
National Institute of Standards and Technology

At the National Institute of Standards and Technology (NIST), we have been developing methods to improve the temperature measurement accuracy of semiconductor materials undergoing high-temperature thermal processing. Our goal is for accuracies of 2 ºC in the range from 700 ºC to 1000 ºC. We have demonstrated new methods for calibrating lightpipe radiation thermometers (LPRTs) against blackbodies with an uncertainty of 0.2 ºC (k = 1). A more challenging issue is how to achieve accurate traceable temperature measurements in process environments. We have studied two approaches: *in-situ* calibration of the LPRT against a thin-film thermocouple test wafer; and making *model-based* corrections to spectral radiance temperatures using an LPRT calibrated against a blackbody. We have achieved uncertainties of 2.3 ºC and 3.5 ºC for the two methods, respectively. While the work specifically addresses a semiconductor application, the approaches have general applicability for achieving reliable, traceable temperature measurements using LPRTs in other material processing and manufacturing environments.

1. Introduction

Recently, many advances have been made in semiconductor metrology. This is evident in the plans by the industry to achieve 100 nm line widths by 2005 [1]. An important growing sector of this industry is rapid thermal processing (RTP) for such purposes as chemical vapor deposition, physical vapor deposition, oxidation, annealing, silicidation, and oxide-etch processes. Compared to the traditional batch processing of silicon wafers, single-wafer RTP can offer advantages of higher ramp rates, shorter processing times, tighter ambient control, and shorter cycle times. Accurate temperature measurement and control during RTP processing is crucial in achieving high throughput and consistent high quality. However, along with the advantages of RTP also come some challenges of making accurate temperature measurements. First, stray light from the source bouncing off reflective surfaces can provide extraneous unwanted signal into the radiometer. In addition, temperature variations with time and with wafer location can complicate the temperature measurement process and can increase the uncertainty of the temperature measurement. Finally, changes in optical properties of the wafer and other parts of the chamber can affect the temperature measurement.

At the National Institute of Standards and Technology (NIST), over the past six years we have been investigating methods of increasing the accuracy of temperature measurement using lightipipe radiation thermometers (LPRTs) in the NIST RTP test bed. Our goals were to achieve 2 ºC in temperature accuracy and 0.5 ºC in temperature repeatability on a silicon wafer. These goals were based on requirements of the International Technology Roadmap for Semiconductors (ITRS). Implicit in the mission of NIST and our RTP temperature project is the task of developing high quality measurement standards and establishing a calibration system whereby others in the United States can derive their temperature traceability. Although NIST cannot and will not dictate to any user community how to define or set traceability standards, the mission of NIST is "to develop and promote measurement, standards, and technology to enhance productivity, facilitate trade, and improve the quality of life." [2] To this end, we are committed to establishing a national protocol for calibration of LPRTs using stable blackbodies in the temperature range of 700 ºC to 1000 ºC traceable to the International Temperature Scale of 1990 (ITS-90).

In this paper, the LPRTs and the sodium heat pipe blackbody (Na-HPBB) used in the calibration process will be introduced. Next, the calibration and characterization methods of the LPRTs will be described. The two approaches, the *in-situ* calibration of the LPRTs and the model-based method, will be explained. Finally, a discussion of the application of LPRTs in an environment outside of the calibration laboratory will be presented.

2. Lightpipe Radiation Thermometers

Lightpipe (LP) sensors are attractive in temperature monitoring applications for at least four reasons. First, the noncontact and nondestructive nature of the LPs does not alter or destroy the original surface. Second, the LPs provide immunity from shock, vibration, and other adverse environments, such as chemical, thermal, and electromagnetic interference. Third, LPs are very convenient especially in confined areas and can be placed very close to a target if desired. Fourth, LPs are safe even in high voltage areas and in ionizing plasma fields.

The LPRT systems used at NIST in Figure 1 consist of a high-quality sapphire crystal LP linked via flexible quartz fibers to a silicon detector operating in the near infrared. Besides the detector, the control box contains the optics and the electronics necessary to digitize the measured signal and to convert it into the appropriate spectral radiance temperature. The sapphire rod is enclosed in a concentric sapphire sheath for protection and mechanical stiffness.

Figure 1. Photograph of LP.

The LPs used in our studies are of varying lengths, but they are about 2 mm in diameter. The sapphire sheath that surrounds the LP has a typical outer diameter of about 4 mm. In normal operation for measuring the spectral radiance temperature, the LPs are connected to a 1 mm diameter quartz fiber-optic cable.

3. Sodium Heat Pipe Blackbody Source

The main inconel cavity of the sodium heat pipe blackbody (Na-HPBB) shown in Figure 2 is 25 mm in diameter and 48 cm in length, whereas its aperture opening is 22 mm in diameter. Surrounding the cylindrical cavity is a 90 mm diameter tube, which contains the sodium liquid/vapor. A condensing tube at the rear of the blackbody allows the metal vapor to liquefy back into the tube and at the same time serves as the conduit by which the tube is pressurized with helium. The Na-HPBB temperature, which is measured by a gold-platinum (Au/Pt) thermocouple (TC), is computer-controlled by regulating the pressure of the helium. Three type S thermocouples monitor the temperature in three zones along the cavity. These temperatures are used in feedback to control the helium pressure through the control software. Using the Au/Pt TC links the Na-HPBB temperature to the ITS-90.

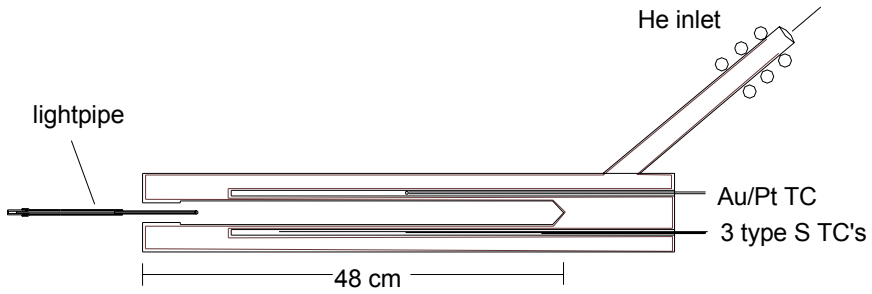

Figure 2. Schematic of Na-HPBB.

4. LPRT Calibrations

On a routine basis, the LPs were calibrated against the Na-HPBB before and after measurements. The LPs undergoing calibration were visually inspected for dirt, and their tips were cleaned with a tissue wiper or a cotton swab saturated with ethyl alcohol. After the Na-HPBB came to a stable temperature and did not vary more than 0.030 °C, the LP was rapidly inserted into the Na-HPBB, measurements of the LPRT indicated temperature were recorded, and the LP was removed before it was heated up significantly. The measurement usually took about 5 s to 10 s and will be referred to as a *cold* calibration. Before and after their use in our test bed experimental studies, a set of LPs was calibrated, and the temperature of the Au/Pt TC was recorded. For each LP, three measurements were averaged and the difference, the average temperature minus the TC temperature, was recorded as the offset temperature. The temperature of the Na-HPBB was then increased to the next temperature, and the whole procedure was repeated.

After use in the RTP test bed for about a month, the LPs were calibrated again to check for variability during use. In Figure 3, typical calibrations of four LPs are shown for a period of one year. Variations during this period of time were less than 1 ºC for all four LPs. Uncertainties for the LPRT calibration using the Na-HPBB are provided in Table 1. The total standard uncertainty (k=1) is 0.19 ºC or about 0.2 ºC.

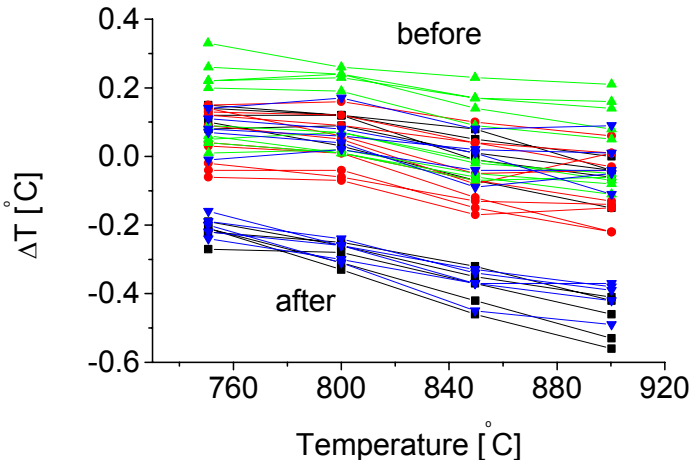

Figure 3. Calibration in the *cold* mode of all LPs with Na-HPBB over a period of one year, including calibrations before and after temperature measurements in the RTP test bed.

Table 1. Uncertainties in units of °C (k = 1) for Na-HPBB calibration of LPRTs at 700 ºC.

Factor	Uncertainty
Na-HPBB radial uniformity	0.18
Na-HPBB length uniformity	0.06
LP noise	0.01
LPRT short-term drift	0.02
Total	0.19

When the LPs were visually dirty (with carbon deposits or other contaminants), or when the LP response in RTP measurements or calibration had dramatically changed, the LPs were cleaned using a flame cleaning procedure. With the outer sheath removed, the LP was first wiped with acetone and ethanol and then heated with an oxygen-methane flame to remove any dirt. Care was exercised to heat the LP slowly and uniformly in order to avoid damage of the LP.

After the LPs had been cleaned through the flaming process, or after the LPs were returned from the factory calibration, the sensor factor settings needed to be adjusted. The adjustment was performed by changing the LP sensor factor setting until the LP indicated reading was within

0.02 °C of the Au/Pt TC reading for the Na-HPBB at the highest calibration temperature, 900 °C. A few LP temperature readings were obtained for repeatability. The LP sensor factor setting was then recorded and then stored for the remainder of the calibration procedure and for future LP measurements. It should be noted that after the LP was cleaned and calibrated, it remained attached to the LPRT until the next flame cleaning was required.

5. LPRT Characterizations

LPRT calibrations are performed using the NIST Na-HPBB. The LPRTs are characterized for target size using the point-spread response (PSR) facility and for absolute spectral response (ASR) using the spectral comparator facility (SCF). Following are summaries of the temperature calibration, PSR and ASR characterizations, and the temporal stability of the LPRTs. A list of recommendations for proper calibration of LPRTs is presented in Appendix A.

5.1. Point spread response

The effective target area on a silicon wafer viewed by the LPRT was determined in the PSR facility. Attached to a precision x-y stage, the LP was translated under computer control in a vertical plane to measure the radiation emanating from a small stationary lamp bulb. The normal distance from the source to the vertical LP plane was carefully set to coincide with the corresponding wafer-to-LP tip gap separation distances in the NIST test bed. From the resulting radiance distribution, the wafer spot was chosen to be the area that enclosed intensities greater than 1 % of the maximum radiance. This technique was repeated for different lamp-to-LP tip gap separations. The contours of the PSR measurement shown in Figure 4 indicate the fraction (with 1.00 being equal to 100 %) of the maximum radiance measured at the origin of the vertical plane in which the LP is translated. This origin is located at the same X and Y location as the lamp bulb. Figure 4 shows that the target size for a gap separation of 12 mm is about 12 mm in diameter for a typical LP. This spot-size information is useful in analytical models for prediction of the effective emissivity and for determination of the corrected LPRT spectral radiance temperature.

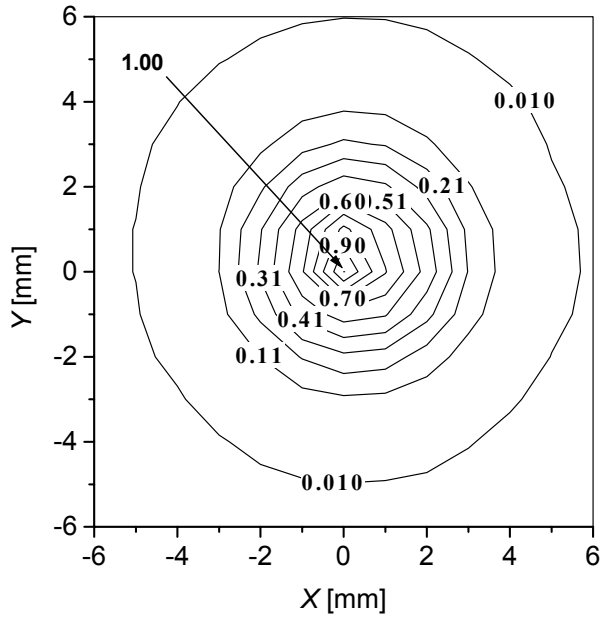

Figure 4. Target size determination from a small lamp bulb 12 mm from front of LP.

5.2. Absolute spectral response

A spectral characterization of the LPRTs was performed using the SCF [3], in which the LP fixed on a linear translation stage was aligned with the center of a monochromator slit and was used to collect the output of a spectrally filtered beam from a quartz-halogen source through the monochromator. This measurement was compared with that using a standard trap detector, calibrated previously with the NIST High Accuracy Cryogenic Radiometer (HACR) [4].

The relative response curves, or the absolute spectral response curves normalized to unity, for three LPs obtained using the SCF are depicted in Figure 5 and are very similar. Based on the full width at half maximum, the peak for all three LPs is centered about an effective wavelength of about 955 nm with a bandwidth of 40 nm. The effective wavelength is critical in the determination of the surface temperature from the LPRT spectral radiance temperature when using the temperature measurement equation. In addition, the effective wavelength is useful in the estimation of the temperature uncertainty. Outside of the 40 nm bandwidth, the relative response quickly decreases four orders of magnitude outside of a bandwidth of about 140 nm. The similarity of all three curves in Figure 5 reveals the consistency and quality of these LPs, which come from two different vendors.

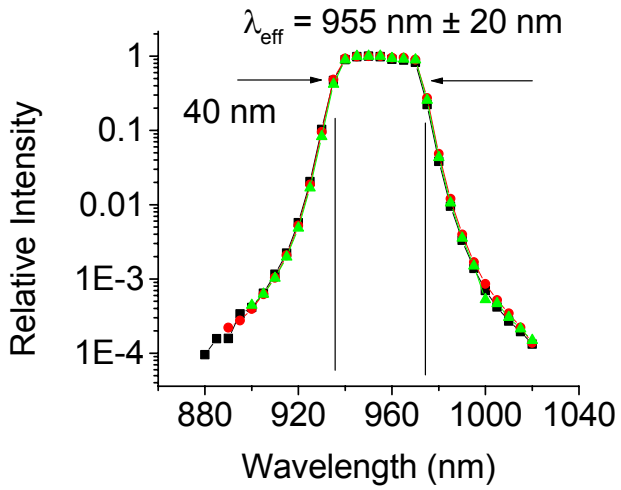

Figure 5. Relative response as a function wavelength for three LPs using the SCF.

5.3. Temporal response

In Figure 6, the temporal stability for a period of 10 min is shown for two LPs, LPRT1 and LPRT2. The results were obtained by irradiation from a helium-neon (HeNe) laser into the LP while it was in the integrating sphere. The resulting variations at room temperature for LPRT1 and LPRT2 were about ±0.06 % and ±0.04 %, respectively. This corresponds to a temperature standard uncertainty at 1000 °C of 0.064 °C and 0.043 °C, respectively.

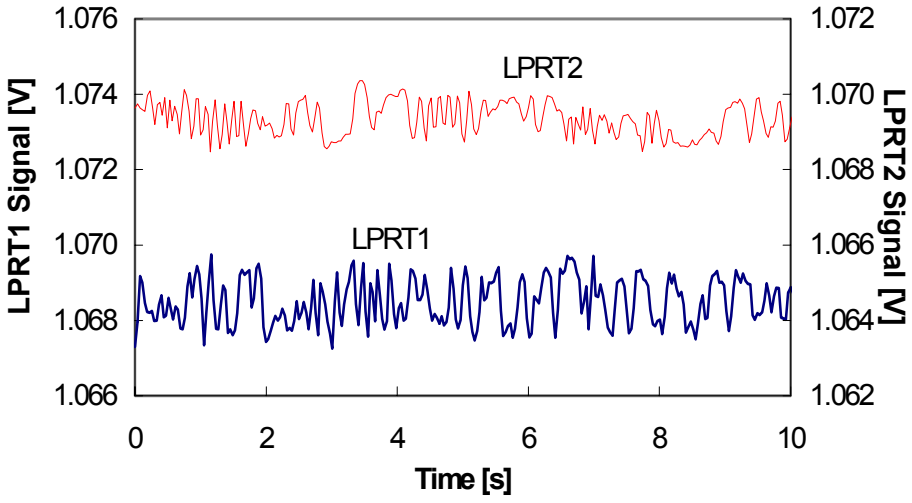

Figure 6. Typical temporal stability for two LPs under stable temperature conditions.

5.4. Optical characterization of LPs

A measure of the LP quality is the radiation scattering from the lateral surface along the length of the pipe. For an ideal LP, the scattering effect will be zero. However, in reality, defects in the manufacturing process can lead to surface imperfections that can cause loss of radiation from the lateral surface. To determine whether such defects are contributing to differences in calibration, two specific studies were conducted with two LPs. Both studies were made by passing a HeNe laser beam (0.95 mW at 637 nm) along the LP and by observing the circumference for irregular patterns.

The first study qualitatively showed a relatively large number of bright spots for LPRT2 at the top of the photograph in Figure 7. This visual study clearly showed the utility of a simple characterization technique to detect scattering defects in defective LPs before calibration and emphasized the need for a more quantitative experiment to determine the radiation loss from the lateral surface due to scattering.

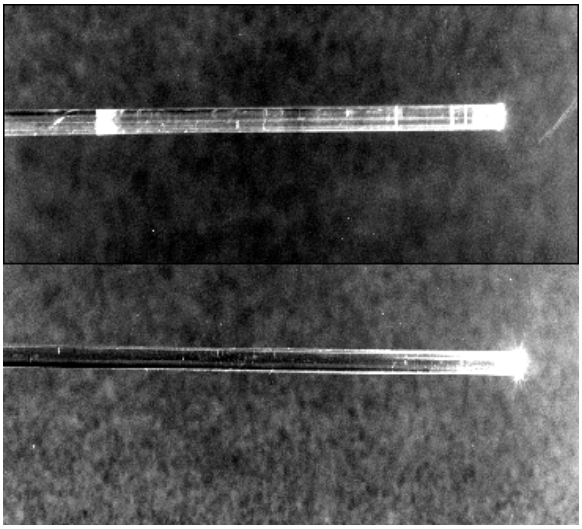

Figure 7. Comparison of LPRT1 (bottom, high quality) and
LPRT2 (top, lesser quality) using HeNe laser.

For the second study, an integrating sphere, about 18 cm in diameter, fitted with a silicon detector was used to measure the radiance of the laser beam *with* and *without* the LP inserted. The laser beam entering the sphere was distributed uniformly on the inner surface of the sphere by multiple reflections. The output of the silicon detector was proportional to the laser power incident on the sphere surface. The low-level current signal from the silicon detector was amplified by a current amplifier, and the output voltage measured by a digital voltmeter. Data recording by the voltmeter was performed by a computer. The two LP positions in the integrating sphere, A and B, in the second study are shown in Figure 8. In Position A, the tip of the LP was positioned in the plane of the integrating sphere aperture. In this position, only the portion of the

radiation transmitted through the length of the LP was distributed onto the integrating sphere surface and was recorded as S_a. In Position B, the LP was inserted inside the sphere cavity with the exposed portion of the sapphire sheath also inside the cavity. The radiation loss from the sheath was also captured, along with the transmitted beam, by the integrating sphere surface and was recorded as S_i. The difference between the readings in Position A and Position B was a measure of the radiation loss through the lateral surface of the LP. Since this radiation loss was less than 1 % of total power, and since intermittent surges in power, lasting several seconds, occurred periodically, the laser measurements were made over a long period of time, and an interval, during which the laser power was stable, was chosen for the analysis.

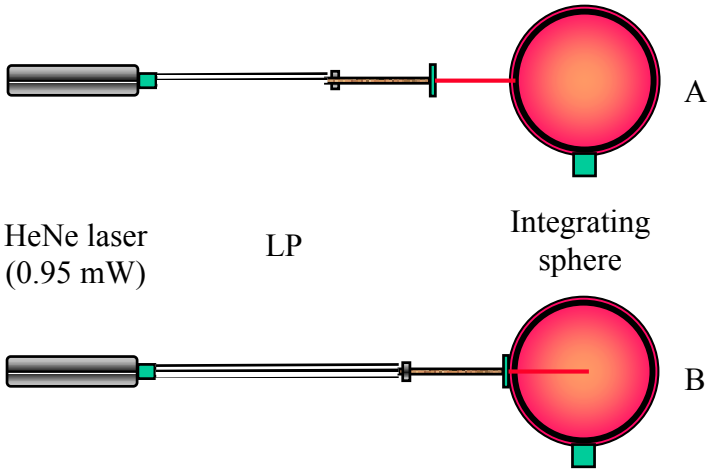

Figure 8. LP positions for measuring transmitted and scattered signals.

Table 2 shows the final results of the measurements for the two LPRTs before and after flame cleaning. The percent difference for LPRT2 is twice as much as that of LPRT1. This correlates to the photograph in Figure 7 where the scattering for LPRT2 is evidently much more than that LPRT1. For all measurements, the dark signal, which was the measured signal taken without the laser and with the integrating sphere aperture covered, was less than 0.001 mV.

Table 2. Summary of LP measurements in the integrating sphere.
(1: LPRT1; 2: LPRT2)

Before or After cleaning	LP ID	Position		Difference
		S_a [V]	S_i [V]	[%]
Before	1	1.04356	1.04803	0.43
Before	2	1.08129	1.09079	0.88
After	1	1.06788	1.06901	0.11
After	2	1.06654	1.06947	0.27

6. *In-situ* calibration of LPRTs

The NIST RTP test bed utilizes quartz-halogen lamps to heat the wafer. A quartz window separates the lamp region from the wafer processing region. Below the quartz window, the silicon wafer is situated on ceramic pins and is shielded from stray radiation by guard surfaces. A detailed description of the test bed is reported in Appendix B. The test bed was suited for conducting an *in-situ* calibration of the LPRTs. Comparisons of the LPRT temperatures with the thin-film thermocouple (TFTC) temperatures can be easily performed in the test bed at the center location and at an offset location. The results of these comparisons indicate how well a direct comparison between the LPRT and TFTC temperatures can be performed.

Figure 9 shows a comparison between the temperatures measured by the thermocouple combination (T_{tc}) and those measured by the LPRT (T_λ) for a diffuse and a specular shield. The measurements were made near the center of the wafer and with a wafer/shield spacing of 12.5 mm. Results using the diffuse shield are shown as diamonds and results using the specular shield are shown as squares. The values of $T_{tc}-T_\lambda$ for the specular shield are 2.5 °C ± 2.1 °C; this demonstrates that with such a chamber environment, the blackbody-calibrated LPRT will read the correct temperature to within this amount. The values of $T_{tc}- T_\lambda$ for the diffuse shield are larger. This is expected, because the reflectance of the specular shield ($\rho = 0.993$) is higher than that of the diffuse shield ($\rho = 0.799$). So, the ε_{eff} for the specular shield is expected to be larger. For both the specular and diffuse shields, the temperature-measurement accuracy of the LPRT will be improved by *in-situ* calibration, which corrects for the $T_{tc}-T_\lambda$ values observed.

The curves shown represent the temperature difference expected for ε_{eff} values of 0.91 and 0.98. The ε_{eff} takes into account irradiation by other surfaces in a cavity and is defined as the ratio of the radiant energy leaving the wafer by emission and reflection to that of a blackbody at the same temperature. The ε_{eff} values were chosen so that the curves would best fit the data. The slope of the data in Figure 9 is clearly larger than that of the curves.

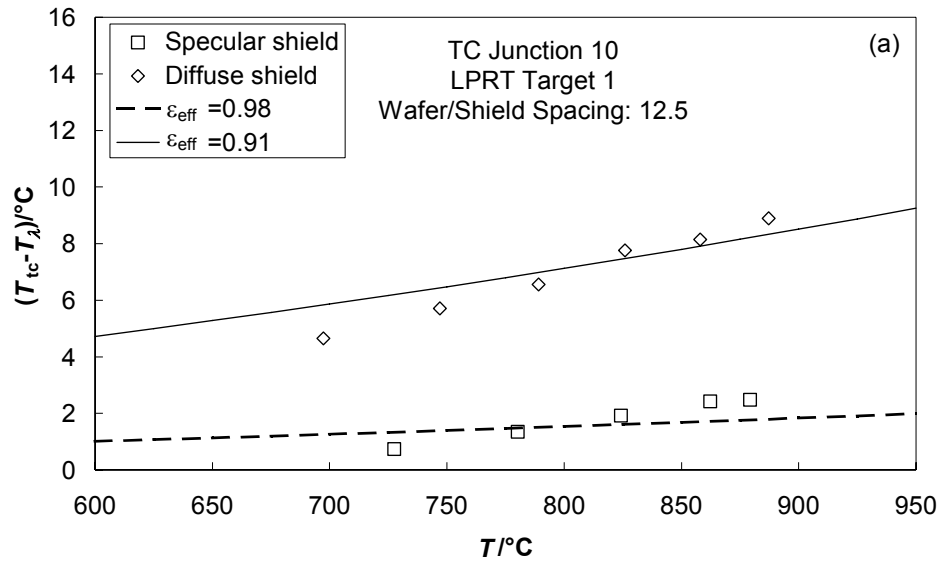

Figure 9. Values of T_{tc} - T_{λ} near wafer center for a gold specular shield (reflectance $\rho = 0.993$) and a gold diffuse shield ($\rho = 0.799$).

Figure 10 shows the effects on $T_{tc}-T_{\lambda}$ of changing the wafer/shield spacing. For this plot, the specular shield was used. While the results for spacings of 12.5 mm and 15.5 mm are identical to within the resolution of the measurements, the values for $T_{tc}-T_{\lambda}$ increase as the spacing is decreased from 12.5 mm to 6 mm. This effect can be explained by the optical perturbation on ε_{eff} of the LPRT target area caused by the presence of the LP, which has a much smaller reflectance ($\rho = 0.075$) than the shield. Because the LP occupies a large solid angle of the field-of-view as seen from a point on the wafer when the wafer is close to the shield, an *in-situ* calibration should be performed with the same spacing as in the application.

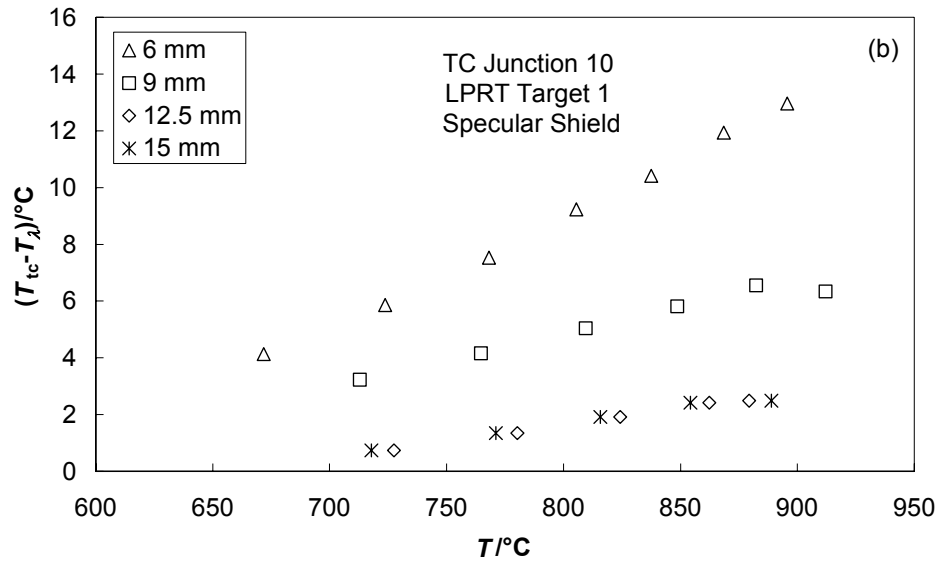

Figure 10. Values of T_{tc} - T_λ near wafer center for four different wafer/shield spacings.

Evaluation of uncertainties were analyzed based on guidelines provided by the International Organization for Standardization [5]. The measurement uncertainties are given below in Table 3. The coverage factor for the uncertainties is k=1. The total uncertainty for the comparisons between the LPRT and the NIST TFTC calibration wafer includes all components in the table, but that for the *in-situ* LPRT calibration against the thermocouples excludes the blackbody/LPRT calibration uncertainty. Both uncertainty totals are calculated by adding their components in quadrature.

The dominant uncertainty arises from the physical separation of 1.4 cm between the TFTC junctions and the center of the LPRT target. The uncertainty estimate of 2.0 °C was based on the assumption of a uniform temperature gradient in this separation. [6, 7] However, no correction for temperature gradients was ever applied to the calibration measurements. Other measurement uncertainties were from temperature fluctuations and long-term temperature drift of the wafer while in steady state, thermocouple calibration uncertainties, LPRT calibration uncertainties, and instrument uncertainties for temperature measurement with the thermocouples and LPRTs. The standard uncertainty for the *in-situ* LPRT calibration is 2.3 ºC.

Table 3. Measurement uncertainties for *in-situ* LPRT calibration (k=1).

Component	U/°C
TFTC calibrations	0.4
Thermocouple emf measurements	1.0
LPRT calibrations	0.2
LPRT measurements	0.1
Wafer temperature fluctuations	0.4
Wafer Temperature drift	0.1
Junction/target temperature difference	2.0
Total	2.3

7. Model-based compensation for effective emissivity

The comparison of the TFTC temperature measurements (T_{TFTC}) and the model-corrected LPRT measurements of wafer temperature (T_{RAD}) is summarized in Figure 11 as a function of wafer temperature for selected gap separations and for chamber configuration with a specular or diffuse shields of reflectance 99.3 % or 79.9 %, respectively. The temperature difference is larger for the smaller separations and shows a positive dependence with increasing wafer temperature that is more pronounced with the smaller separations. Since there is higher confidence in the 5-region effective emissivity model results for the larger separations, the data for the 12.5-mm gap condition is thought to represent a meaningful comparison of the TFTC and LPRT measurements. For this separation, the results with the specular and diffuse shields nearly overlap. The comparison difference shows that LPRT corrected temperatures are systematically higher than the TFTC by approximately 3 °C.

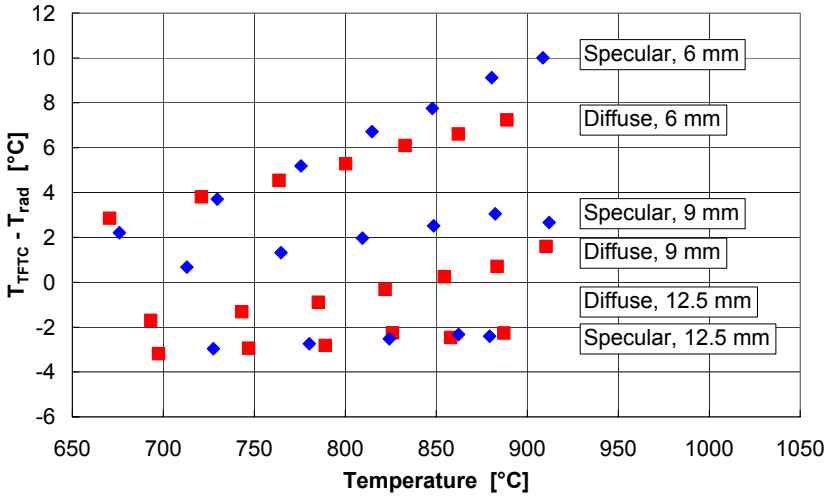

Figure 11. Comparison of TFTC and model-corrected LPRT wafer temperatures with the specular (99.9 % reflectance) and diffuse (79.9 % reflectance) cold shields for gap separations of 6 mm, 9 mm, and 12 mm.

Estimates for the uncertainties for the TC and LPRT measurements are shown in Table 4. The major contributor to the LPRT measurement uncertainty is the ε_{eff} uncertainty. For the specular shield, the ε_{eff} is quite high. If we conclude that the uncertainty of the model ε_{eff} amounts to 0.03 emissivity units, the corresponding uncertainty due to the ε_{eff} uncertainty is about 2.0 °C. The second major contributor is due to the temperature difference between the LPRT target and the TC amounting to 2.0 °C. The total TC and LPRT measurement uncertainties (k=1) are 3.5 °C and 0.4 °C [1], respectively.

Table 4. Temperature uncertainties (k=1) [°C] for comparison of LPRT and TC measurements.

Calibration	0.2
Effective emissivity	2.0
Junction/target temperature difference	2.0
Temperature fluctuations	0.4
Temperature drift	0.1
LPRT display	0.1
Subtotal	3.5

8. Using calibrations in industrial applications

We have shown that LPRTs can be calibrated against a stable blackbody with a very low uncertainty. At NIST, we have also used the calibrated LPRTs in our test bed with acceptable

uncertainties by comparing the LPRTs directly *in-situ* with TFTC wafers and by implementing *model-based* algorithms to determine the wafer temperature.

Applying calibrated LPRTs in an industrial or factory application is more complicated and requires more analysis for determination of temperature, as well as establishing uncertainty limits *and* traceability. In this section, we present two issues associated with using LPRTs in applications outside of a well-controlled laboratory environment. First, caution is given to those who use factory calibration data without consideration of what the data represents. Second, a differentiation is made between two types of calibration for LPRTs. The main recommendation is to calibrate in the same fashion as the application.

Three LPs from different vendors, using the factory-set sensor factors, were calibrated using the Na-HPBB as soon as they were received at NIST. The differences between the LPRT indicated temperatures in the *hot* mode using factory calibrations and the actual temperatures measured with the Au/Pt TCs in the Na-HPBB are shown in Figure 12. The results show that for the LPRT2 and the LPRT3, the variations among each set of four LPs can be high as 7.6 ºC, while for the LPRT1 such variations are less than 1.6 ºC.

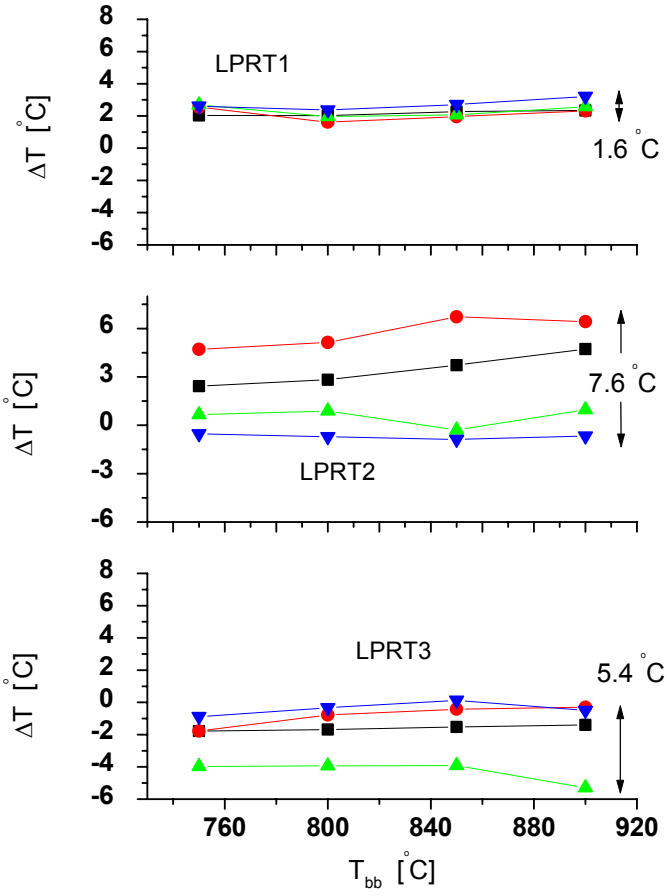

Figure 12. Differences between factory and NIST *hot* calibrations for three LPRTs.

In the Na-HPBB, time histories of all of the LPs are shown in Figure 13. After the LP is inserted into the Na-HPBB for a few seconds, the LPRT indicated temperature initially remained fairly constant, dipped, and then rose above the initial temperature to a steady temperature. *Cold* calibrations were performed in the initial period when the temperature was still constant, while *hot* calibrations were performed after the Na-HPBB was stable during the second temperature rise. Although most LPRTs behaved in this manner, other patterns have been observed. However, in general, there was a constant plateau during the first 30 s or 1 min (*cold*) and again after 5 min (*hot*) from insertion.

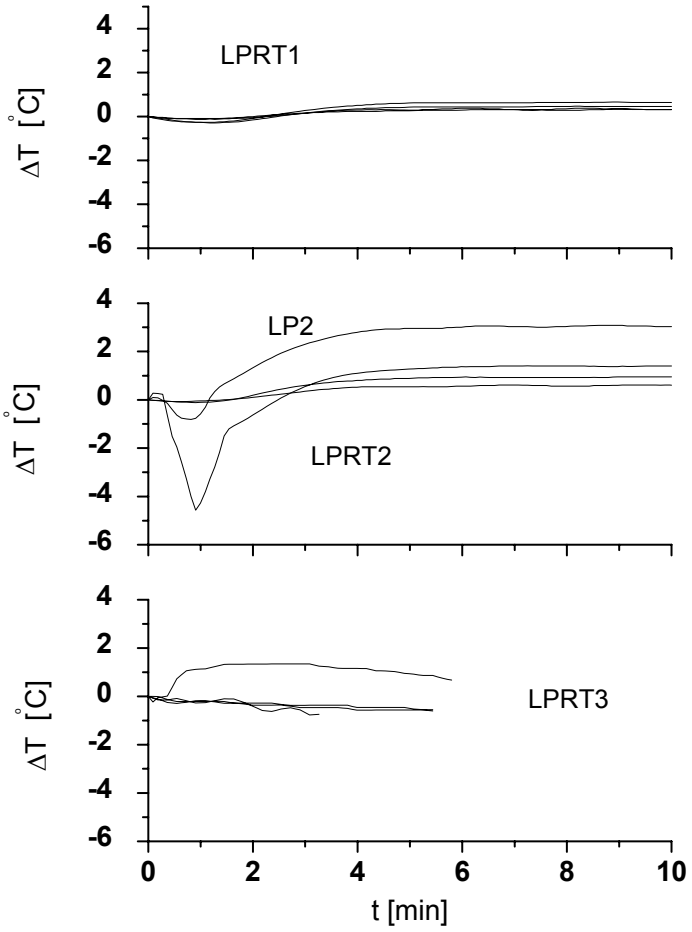

Figure 13. *Hot-cold* calibrations of four LPs from three LPRTs for 10 min with the Na-HPBB at 850 °C.

Significant differences exist between *hot* and *cold* LP calibrations in Figure 13 of up to 2.5 °C for LPRT2, while only modest differences of up to 0.7 °C for LPRT1 were exhibited. Visual

defects as well as the ratios of the scattered signal to the transmitted signal have direct relationships with the amount of thermal leakage as measured by the net temperature rise in 10 min. The visual defects and transmission measurements both have a strong correlation with the difference between *hot* and *cold* LP calibrations. LPRT2-LP2 exhibited a large difference of 2.5 °C in Figure 13 and a large slope in Figure 12. It also showed the most visual defects from the optical characterization. On the other hand, LPRT1-LP2 showed only a difference of 0.5 °C in Figure 13 and a slight slope in Figure 12. This LP was relatively clear of visual defects from the optical characterization. In order to make accurate LP temperature measurements, it is necessary to understand the accuracy of factory calibrations, the difference between *hot* and *cold* calibrations, and the importance of visualization and measurement techniques in defect detection for LPs.

9. Conclusions

We have calibrated LPRTs against a stable blackbody with a standard uncertainty (k=1) of 0.2 ºC. We have also performed *in-situ* calibrations of LPRTs with an uncertainty (k=1) of 2.3 ºC in an RTP test bed against wire/TFTC combinations calibrated on the ITS-90. Using a model-based approach, we have measured test bed temperatures using the calibrated LPRT with an uncertainty (k=1) of 3.5 ºC. While this work specifically addresses a semiconductor application, the approaches have general applicability for achieving reliable, traceable temperature measurements using LPRTs in other material processing and manufacturing environments.

10. Bibliography

1. Semiconductor Industry Association, International Technology Roadmap for Semiconductors: 2000 Update, 1999.
2. NIST, http://www.nist.gov/public_affairs/nist_mission.htm, 2002.
3. T.C. Larason, S.S. Bruce, and A.C. Parr, Spectroradiometric Detector Measurements, *NIST Special Publication* 250-41, 1998.
4. T.R. Gentile, J.M. Houston, J.E. Hardis, C.L. Cromer, and A.C. Parr, The NIST High Accuracy Cryogenic Radiometer, *Applied Optics*, vol. 35, p. 1056, 1996.
5. ISO, Guide to the Expression of Uncertainty in Measurement, International Organization for Standardization, Geneva, Switzerland, 1993.
6. C.W. Meyer, D.W. Allen, D.P. DeWitt, K.G. Kreider, F.J. Lovas, and B.K. Tsai, ITS-90 Calibration Of Radiometers Using Wire/Thin-Film Thermocouples In The NIST RTP Tool: Experimental Procedures And Results, *7th International Conference on Advanced Thermal Processing of Semiconductors – RTP'99*, pp. 136-141, 1999.
7. K.G. Kreider, D.P. DeWitt, C.W. Meyer, and V.P. Scheuerman, Calibration of Lightpipe Radiation Thermometers in a RTP Tool at 1000 ºC, *8th International Conference on Advanced Thermal Processing of Semiconductors – RTP'2000*, pp. 65-70, 2000.
8. P.Y. Barnes, E.A. Early, and A.C. Parr, Spectral Reflectance, *NIST Special Publication* 250-48, 1998.

11. Acknowledgments

The authors gratefully acknowledge the collaboration from our project colleagues, Dr. Ken G. Kreider and Mr. William Kimes of the Process Measurements Division at NIST.

12. Appendix A – NIST Recommendations for LPRT Calibrations

Based upon our LPRT calibration and characterization experiences at NIST, we offer the following recommendations for users of LPRTs in calibration or measurement applications:

1. *Visually inspect the LP first*. Before any calibration or measurement is performed, the LP should be inspected visually for defects, such as macroscopic chips and nicks.
2. *Understand the factory calibration*. When factory calibration data is available, the user should verify whether the factory calibrations were performed using the *hot* or *cold* calibration mode. If possible, the LP calibrations should then be checked using blackbody sources.
3. *Characterize the LPRT*. The LPRTs should be characterized spectrally, spatially, and temporally with available resources.
4. *Minimize lateral scattering*. Wherever possible, a method to minimize lateral scattering through the LP, such as a water-cooled sleeve, should be used for *cold* calibrations. This will ensure that extraneous radiation is eliminated in LP calibrations and that the LP remains at a cold temperature.
5. *Calibrate the LPRT as it will be used*. The cardinal rule of LPRT calibrations is to calibrate in the same manner in which it will be used. LPs are operated *hot* or *cold* in different RTP tools.
6. *Calibrate the LPRT using blackbodies that are traceable to a National Measurement Institute*. For highest accuracy, the LPRT should be calibrated using blackbodies traceable to a National Measurement Institute, such as NIST.
7. *Calibrate before and after use*. Immediately before and after LP use, the LPs should be calibrated to check for any systematic drift. If there is any significant change in calibration, the LPs should be inspected again for any damage or contamination during use and moving of the LPs.

These practical principles have been formed from our experience with calibrations and measurements of LPs from several vendors. Following these guidelines wherever possible can ensure highly accurate LP calibrations and temperature measurements on the ITS-90.

13. Appendix B – Description of NIST RTP Test Bed

The walls of the RTP chamber shown in Figure 14 were made of stainless steel. Heating was produced by an array of 24 2-kW quartz-halogen lamps located 15.0 cm above the chamber. The lamps were surrounded on the top and sides by a gold-plated housing with a hexagonal

geometry, which reflected stray radiation down into the chamber. The wafer, which was supported by three 2-mm diameter alumina rods, was located approximately 3.6 cm below the quartz plate. A 26.7-cm diameter water-cooled copper plate was located underneath the wafer. Atop the plate was a 1-mm thick brass reflective shield of the same diameter, which was held tight against the copper plate by a vacuum. The total hemispherical reflectance of the reflective shields were measured by the NIST Optical Thermometry and Spectral Methods Group using the techniques described in [8].

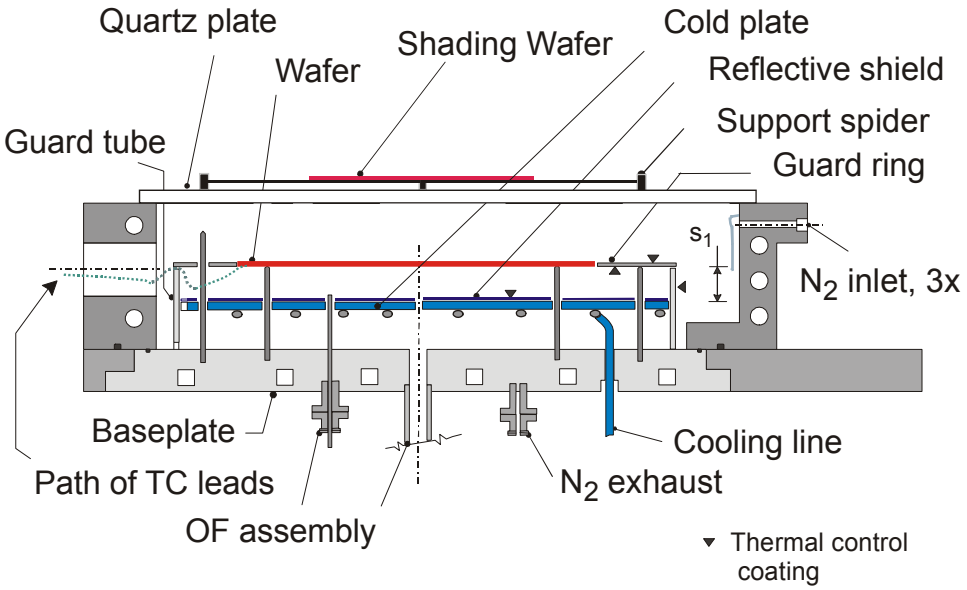

Figure 14. The NIST RTP test bed.

Five holes were drilled through the copper plate to allow for insertion of the LPRTs. One hole of 4 mm diameter was in the center of the plate and the other four were of 7 mm diameter and located at a radius of 5.4 cm from the center of the plate and at equal angles from each other. The bottom reflective shields had similar holes, except that all holes for LPRTs in the diffuse shield were of 4 mm diameter. In addition to the holes described above, three 2.2-mm diameter holes were drilled through the copper plate and reflective shields at a radius of 7.5 cm and at equal angles to allow for the insertion of the alumina rods supporting the wafer. The copper plate was surrounded by a quartz guard tube with 5 mm thick walls, an inner diameter of 26.9 cm and 4.5 cm high as shown in the figure. The guard tube was coated on the outside with platinum. On top of the guard tube rested a 1-mm thick quartz guard ring with an outer diameter of 30 cm and inner diameter of 20.2 cm as shown; this ring was coated with platinum on the bottom side. This design provided an enclosure underneath the wafer that was almost completely shielded from stray radiation and which was surrounded on the top and sides by platinum-coated reflective shields and on the bottom by a gold-coated reflective shield. Allowing the wafer/shield spacing to be adjustable by changing the alumina rods permitted study of the dependence of ε_{eff} on this parameter to provide data to verify models for characterizing the reflective enclosure.